CELL BIOLOGY

PBRM1 and the glycosylphosphatidylinositol biosynthetic pathway promote tumor killing mediated by MHC-unrestricted cytotoxic lymphocytes

Bridget L. Menasche[1]*, Eric M. Davis[1]*, Shifeng Wang[1,2]*, Yan Ouyang[1], Suzhao Li[3], Haijia Yu[1,4], Jingshi Shen[1†]

Major histocompatibility complex (MHC)–unrestricted cytotoxic lymphocytes (CLs) such as natural killer (NK) cells can detect and destroy tumor and virus-infected cells resistant to T cell–mediated killing. Here, we performed genome-wide genetic screens to identify tumor-intrinsic genes regulating killing by MHC-unrestricted CLs. A group of genes identified in our screens encode enzymes for the biosynthesis of the glycosylphosphatidylinositol (GPI) anchor, which is not involved in tumor response to T cell–mediated cytotoxicity. Another gene identified in the screens was *PBRM1*, which encodes a subunit of the PBAF form of the SWI/SNF chromatin-remodeling complex. *PBRM1* mutations in tumor cells cause resistance to MHC-unrestricted killing, in contrast to their sensitizing effects on T cell–mediated killing. PBRM1 and the GPI biosynthetic pathway regulate the ligands of NK cell receptors in tumor cells and promote cytolytic granule secretion in CLs. The regulators identified in this work represent potential targets for cancer immunotherapy.

INTRODUCTION

Cytotoxic lymphocytes (CLs) are subtypes of immune cells capable of detecting and killing tumor and virus-infected cells (*1*, *2*). Current cancer immunotherapy mainly harnesses the antitumor activities of cytotoxic T cells, effectors of the adaptive immune system (*2*–*5*). T cells detect transformed cells by using their T cell receptors to recognize tumor neoantigens displayed on the major histocompatibility complex (MHC) class I proteins of tumor cells (*6*–*8*). T cell–based therapies such as checkpoint inhibitors substantially extend the survival of a subset of patients with cancer (*3*–*5*, *9*). Many tumors, however, are unresponsive to checkpoint therapies, possibly because of defects in presentation of tumor antigens on MHC class I (*2*). Moreover, tumor cells that initially respond to checkpoint inhibitor therapies often develop acquired resistance, resulting in tumor relapses (*2*, *4*). Therefore, additional immunotherapeutic strategies are needed to achieve sustained clinical benefits in a larger patient population.

Another class of tumor-killing CLs are MHC-unrestricted CLs, which include natural killer (NK) cells, effectors of the innate immune system, and NK-like cell lines (*10*–*14*). Unlike T cells, MHC-unrestricted CLs kill tumor or virally infected cells without requiring prior activation by MHC-presented antigens (*6*, *15*, *16*). The absence of MHC class I on target cells serves as a strong activation signal for MHC-unrestricted CLs (*1*, *6*, *10*, *12*, *17*). As a result, MHC-unrestricted CLs are capable of detecting and destroying tumor cells resistant to T cell–mediated attack, holding great promise as mono or combination immunotherapies (*18*, *19*). However, the antitumor activities of MHC-unrestricted CLs have not been translated into significant clinical benefits to patients, likely because of escape mechanisms evolved by tumor cells to circumvent killing (*19*, *20*). To improve the efficacy of MHC-unrestricted CLs in immunotherapy, it is critical to identify genes controlling the response of tumor cells to cytotoxicity.

In this work, we performed genome-wide genetic screens to uncover tumor-intrinsic genes that regulate tumor killing by MHC-unrestricted CLs. Our screens identified a large number of regulators that either promote or inhibit the response of tumor cells to killing. The screens isolated known mediators of NK cell–mediated killing, but most of the identified genes were not previously linked to tumor killing. Multiple top-ranking genes in the screens belong to the glycosylphosphatidylinositol (GPI) anchor biosynthetic pathway, which is not involved in T cell–mediated killing. Further analyses revealed that the GPI biosynthetic pathway is required for the activation and cytolytic granule secretion of CLs. Another critical regulator identified in the screens was PBRM1, a component of the SWI/SNF chromatin-remodeling complex. Notably, PBRM1 promotes the killing of tumor cells by MHC-unrestricted CLs, in contrast to its inhibitory activity in T cell–mediated killing. Thus, PBRM1 plays opposite roles in MHC-restricted and MHC-unrestricted cytotoxicity. Like the GPI biosynthetic pathway, PBRM1 promotes cytolytic granule secretion in CLs. The factors identified in this work could represent potential targets for cancer immunotherapy.

RESULTS

Identification of positive regulators of TALL-104–mediated tumor killing

We developed a tumor-killing platform using TALL-104 cells, a clinically relevant CL cell line exhibiting robust MHC-unrestricted cytotoxicity against human tumors (*14*, *18*, *21*–*23*). Despite the T cell origin of this cell line, TALL-104 cells express NK cell receptors and closely resemble NK cells in recognizing and destroying tumors without prior sensitization (fig. S1) (*14*). Previously, TALL-104 cells have been used in clinical trials to treat patients with cancer (*14*, *18*, *21*–*24*). A major advantage of TALL-104 cells is that they can be readily expanded into large homogeneous populations to meet the demands of genome-wide genetic screens. We observed that TALL-104 cells efficiently killed HAP1 cells (Fig. 1A and fig. S2A),

[1]Department of Molecular, Cellular and Developmental Biology, University of Colorado Boulder, Boulder, CO 80309, USA. [2]Department of Chinese Medicine Information Science, Beijing University of Chinese Medicine, Beijing 102488, China. [3]Department of Medicine, University of Colorado Anschutz Medical Campus, Aurora, CO 80045, USA. [4]Jiangsu Key Laboratory for Molecular and Medical Biotechnology, College of Life Sciences, Nanjing Normal University, Nanjing 210023, China.
*These authors contributed equally to this work.
†Corresponding author. Email: jingshi.shen@colorado.edu

a haploid human cell line derived from chronic myeloid leukemia cells (*25*–*27*). By contrast, primary human cells, including peripheral blood mononuclear cells (PBMCs) and adipose stem cells (ASCs), were resistant to TALL-104–mediated killing (Fig. 1A and fig. S2B), consistent with the ability of CLs to distinguish between tumor and normal cells (*6*–*8*).

To systematically identify tumor-intrinsic genes required for TALL-104–mediated killing, pooled HAP1 cells were randomly mutagenized using retroviral gene-trap insertions (*27*–*29*). The mutagenized HAP1 cells were incubated with TALL-104 cells for four consecutive rounds, in which approximately 50% of the HAP1 cells were killed during each round (Fig. 1B). After the final round of killing, the TALL-104–resistant HAP1 population was harvested, and their gene-trap retroviral insertions were mapped by deep sequencing. The gene-trap insertions were then compared to those of an untreated control HAP1 population to identify significant hits on the basis of the enrichment of inactivating gene-trap insertions.

The haploid genetic screen identified a number of genes that promote TALL-104–mediated killing (Fig. 1C and table S1). Mutations of these genes in target cells caused resistance to TALL-104–mediated cytotoxicity. One gene identified in the screen was *NCR3LG1*/*B7H6*, which encodes an activating ligand for the NK cell receptor NKp30 (Fig. 1C) (*30*). Another hit from the screen was *PVR*/*CD155*, which encodes a ligand for DNAX accessory molecule 1 (DNAM-1), another activating receptor on NK cells (Fig. 1C) (*10*–*12*). Our screen also recovered *IFNGR2*, which encodes the interferon-γ (IFN-γ) receptor critical to NK cell–mediated cytotoxicity (*10*–*12*). Recovery of these known mediators of NK cell cytotoxicity strongly supports the physiological relevance of the screen and further demonstrates that TALL-104 cells resemble NK cells in tumor killing. Most of the hits, however, were not previously linked to CL-mediated killing.

Multiple genes identified in the screen, including *PIGP*, *PIGS*, *PIGL*, and *GPAA1*, encode enzymes responsible for the biosynthesis of the GPI moiety of GPI-anchored proteins (GPI-APs) (Fig. 1C) (*28*). Thus, the GPI anchor biosynthetic pathway is required for tumor cell sensitivity to TALL-104–mediated cytotoxicity. Another top-ranking hit was *PBRM1*/*BAF180*, which encodes a subunit of the PBAF form of the SWI/SNF chromatin-remodeling complex (Fig. 1C) (*31*, *32*). Other genes isolated in the screen encode factors involved in a range of cellular processes including membrane trafficking and gene expression (fig. S3).

Discovery of additional positive regulators of TALL-104–mediated killing in a modifier screen

Since a large fraction of the inactivating gene-trap insertions in the primary screen were within the GPI anchor biosynthetic genes

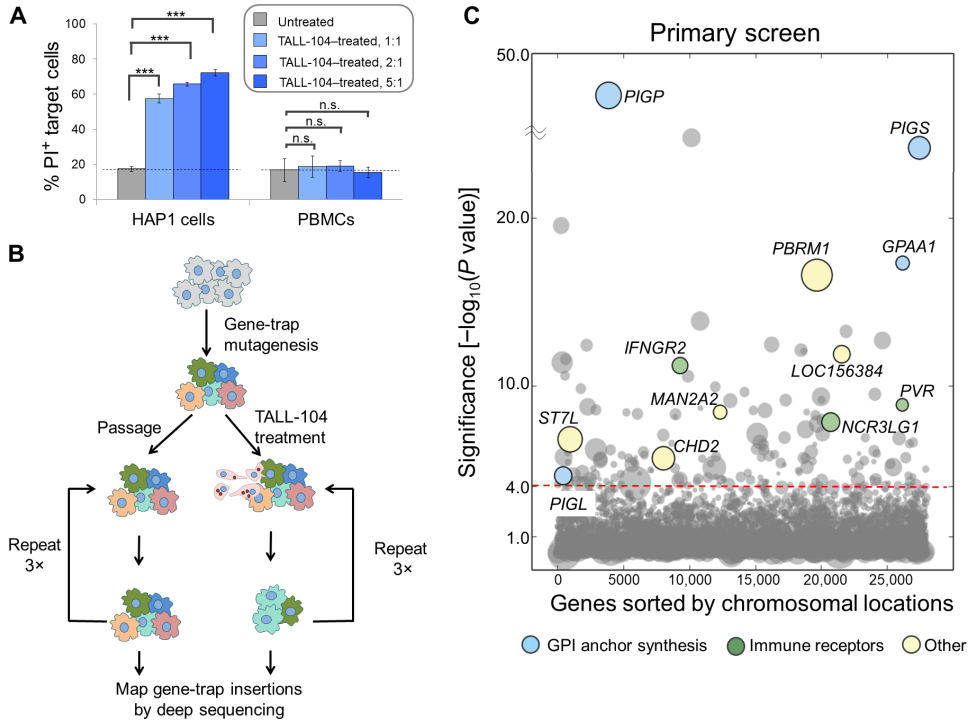

Fig. 1. Identification of positive regulators of TALL-104–mediated tumor killing in a genome-wide haploid genetic screen. (**A**) TALL-104 cells (CLs) kill HAP1 cells (tumor cells) but not normal cells. HAP1 cells and human PBMCs grown on a 24-well plate were treated with the indicated ratios of TALL-104 cells for 8 hours. The cells were stained with propidium iodide (PI) and measured by flow cytometry. Error bars indicate SD ($n = 3$). P values were calculated using Student's t test. ***$P < 0.001$. n.s., $P > 0.05$. (**B**) Illustration of the genome-wide haploid genetic screen aiming to identify tumor-intrinsic genes required for TALL-104 cytotoxicity. (**C**) Bubble graph showing significant hits from the haploid genetic screen. The y axis depicts the $-\log_{10}$ of P values for the gene hits in the TALL-104–selected population as compared to a published unselected control (*62*) using Fisher's exact test. Dashed line indicates the cutoff of significance. We set a P value cutoff of 1×10^{-5} to account for multiple hypothesis testing. In addition, for genes with P values less than 1×10^{-10}, we considered a gene as a hit only if it also had strong enrichment for sense-strand intron insertions based on the binomial test (P value cutoff: 1×10^{-5}). The x axis depicts the chromosomal positions of the genes. The size of a circle is scaled according to the number of unique inactivating gene-trap insertions within the gene. Circles are colored according to the annotated or predicted functions of the gene products. Genes that did not reach the cutoff are shown in gray. Full datasets of the screen are included in table S1.

(table S1), additional regulators might have been masked. To this end, we next performed a genome-scale modifier screen using GPI-deficient HAP1 cells. We used CRISPR-Cas9 genome editing to delete *PIGP*, a key gene in GPI anchor biosynthesis (*28*). Surface expression of the GPI-AP CD59 was abolished (Fig. 2A), confirming the loss of the GPI anchor in *PIGP* knockout (KO) cells. GPI anchor–deficient HAP1 cells were still killed by TALL-104 cells, albeit with a significantly lower efficiency.

The modifier screen using GPI anchor–deficient cells recovered most of the hits from the primary screen including *NCR3LG1*, *PVR*, and *IFNGR2* (Fig. 2, B and C), validating the critical roles of these genes in TALL-104–mediated killing. As expected, none of the genes involved in GPI anchor biosynthesis were recovered in the modifier screen (Fig. 2, B and C; figs. S3 and S4; and table S2). The modifier screen identified many additional genes including *TNFRSF10A* and *TNFRSF10B* (Fig. 2, B and C), which encode TRAIL death receptors known to mediate CL-mediated killing (*6*, *10*). These findings are consistent with roles of death receptors in NK cell–mediated killing. Other genes identified in the modifier screen were not previously linked to tumor killing. Notably, a subset of the genes identified in the primary screen including *PBRM1* were not recovered in the modifier screen (Fig. 2, B and C, and fig. S4), suggesting that these genes might be linked to the GPI biosynthetic pathway in TALL-104–mediated killing.

Previous genetic screens dissected MHC-restricted tumor killing mediated by cytotoxic T lymphocytes (*33*–*35*). Next, we compared the hits from our screens with those from T cell–based screens. The IFN-γ receptor was also recovered in T cell screens (*33*–*35*), in agreement with the role of the IFN-γ pathway in both MHC-restricted and MHC-unrestricted cytotoxicity (*8*, *10*, *12*). However, most of the hits from our genetic screens, including the GPI biosynthetic genes, were not isolated in T cell–based screens (*33*–*35*). Likewise, most genes identified in T cell–based screens were not recovered in our screens. In particular, a large portion of genes identified in T cell–based screens encode regulators of the MHC class I and PD-L1 (programmed cell death 1 ligand 1) pathways (*33*–*35*). As expected, these genes

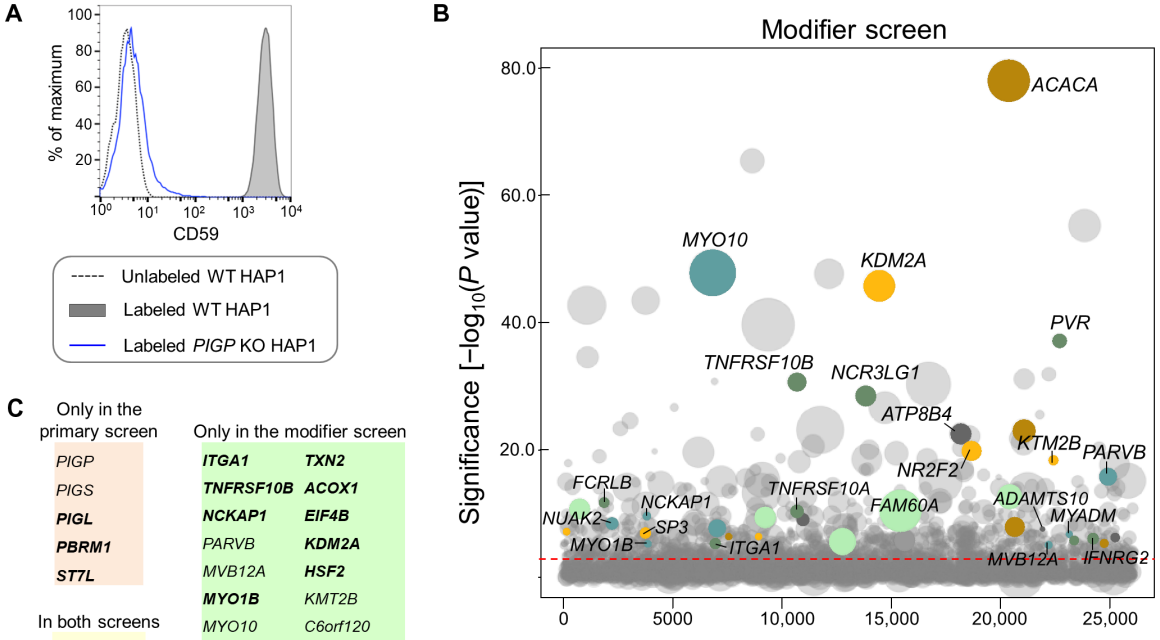

C

Only in the primary screen	Only in the modifier screen	
PIGP	***ITGA1***	***TXN2***
PIGS	***TNFRSF10B***	***ACOX1***
PIGL	***NCKAP1***	***EIF4B***
PBRM1	*PARVB*	***KDM2A***
ST7L	*MVB12A*	***HSF2***
	MYO1B	*KMT2B*
In both screens	*MYO10*	*C6orf120*
PVR	*ACACA*	*GNPDA1*
IFNGR2	***DCAKD***	*MAST4*
TNFRSF10B	***FCRLB***	*ATP8B4*
DCAKD	***TNFRSF10A***	*HES2*
MYADM	*TRIB3*	***NR2F2***
GPAA1	***ADAMTS10***	*ZFAND4*
SP3	*NUAK2*	*FAM183A*
CHD2	*NYX*	***FAM60A***
NCR3LG1	*SLCO5A1*	*LRRC37A11P*

Fig. 2. Discovery of additional positive regulators of TALL-104–mediated killing in a modifier screen. (**A**) Flow cytometry measurements of the surface levels of CD59, a GPI-AP used as a marker for the GPI pathway (CD59 is not involved in CL-mediated killing). *PIGP* KO HAP1 cells were generated using CRISPR-Cas9 genome editing. A lack of surface CD59 in pooled *PIGP* KO cells indicates that the GPI pathway was abolished. WT, wild-type. (**B**) Screen hits from the modifier haploid genetic screen using the *PIGP* KO HAP1 cells. The screen was performed as described in Fig. 1. The *y* axis depicts the $-\log_{10}$ of *P* values for the gene hits in the TALL-104 selected population compared to the unselected control using Fisher's exact test. We set a *P* value cutoff of 1×10^{-5} to account for multiple hypothesis testing. In addition, we considered a gene as a hit only if it also had strong enrichment for sense-strand intron insertions based on the binomial test (*P* value cutoff: 1×10^{-5}). The *x* axis depicts the chromosomal positions of the genes. The size of the circle is scaled according to the number of unique inactivating gene-trap insertions with the gene. Circles are colored according to the annotated or predicted functions of the gene products. Dashed line indicates the cutoff of significance. Genes that did not reach the cutoff are shown in gray. Full datasets are included in table S2. (**C**) Lists of genes identified in the primary and modifier screens. Genes linked to cancer or CL killing are highlighted in bold. Cancer association is based on the COSMIC database.

were not recovered in our MHC-unrestricted screens (Fig. 2C and fig. S4). Notably, although *PBRM1* was also isolated in T cell–based screens of tumor killing (*35*), its function is distinct: PBRM1 inhibits T cell–mediated cytotoxicity but promotes TALL-104–mediated killing (Fig. 1C) (*35*). Thus, PBRM1 plays both positive and negative roles in tumor killing. Together, these findings demonstrate differences between the regulatory networks underlying MHC-restricted and MHC-unrestricted cytotoxicity.

According to gene set enrichment analysis (GSEA) (*36*), the factors identified in our screens belong to multiple KEGG (Kyoto Encyclopedia of Genes and Genomes) pathways and form physical or functional networks (figs. S5 and S6 and table S3). Approximately half of the hits identified in our screens were mutated in human cancers according to the Catalogue of Somatic Mutations in Cancer (COSMIC) database (Fig. 2C). Since these genes do not regulate cell growth (table S4), our data suggest that cancer-linked mutations in these genes may promote tumorigenesis by preventing NK cell–mediated tumor killing.

Identification of negative regulators of TALL-104–mediated tumor killing

Next, we sought to identify tumor-intrinsic genes encoding negative regulators of TALL-104–mediated killing on the basis of depletion of inactivating gene-trap insertions. To accurately calculate gene-trap depletion from a large mutant cell population, we developed gene-trap strand profile (GSP), a scoring metric based on the numbers of unique inactivating (sense) or neutral (antisense) gene-trap insertions within the introns of a candidate gene. A negative GSP score represents the depletion of inactivating gene-trap insertions in a gene, corresponding to a detrimental effect of the gene KO on cell viability (fig. S7, A to C). As a proof of concept, we used the GSP scoring metric to identify the genes essential to the viability or growth of HAP1 cells in the absence of TALL-104 cells. Approximately 1788 essential genes were identified, encompassing all known essential pathways such as translation, transcription, and RNA splicing (fig. S7, D and E, and table S4). This list included virtually all the essential genes identified in previous genetic studies (*26*, *37*), suggesting that GSP scores accurately quantify gene-trap depletions.

Subsequently, we identified genes with significantly negative GSP scores in TALL-104–selected HAP1 cells but not in the passage control population. Mutations of these genes sensitize the tumor cells to TALL-104–mediated killing, leading to the depletion of inactivating gene-trap insertions. Thus, these genes encode negative regulators of tumor killing by TALL-104 cells. One of the negative factors identified in both the primary and modifier screens was CFLAR (CASP8 and Fas-associated death domain protein (FADD)–like apoptosis regulator) (Fig. 3A), a known inhibitor of TRAIL-mediated apoptosis (*38*, *39*). Another negative factor identified in both the primary and modifier screens was MGA, a transcription factor not previously linked to CL-mediated cytotoxicity (Fig. 3A). The ratio of inactivating and neutral gene-trap insertions in *CFLAR* and *MGA* genes was approximately 1:1 in the absence of TALL-104 selection, indicating that *CFLAR* and *MGA* are not essential to cell growth (Fig. 3A). However, their inactivating gene-trap insertions were strongly depleted after TALL-104 selection (Fig. 3A), reflecting the inhibitory roles of these genes in TALL-104–mediated killing. Other negative regulators identified in the screens encompass a range of biological pathways such as TRAIL signaling, transcriptional regulation, and membrane trafficking (Fig. 3, B and C). A group of negative regulators identified in the primary screen were also recovered in the modifier screen (Fig. 3B and fig. S8). Many others, however, were not isolated in the modifier screen (fig. S8 and tables S5 and S6). While a subset of the negative regulators such as CFLAR were also involved in T cell–mediated killing (*33*–*35*), most of the factors were not recovered in T cell–based screens of tumor killing, again highlighting the fundamental differences between MHC-unrestricted and MHC-restricted cytotoxicity.

The GPI biosynthetic pathway is required for the activation and cytolytic granule secretion of MHC-unrestricted CLs

Next, we sought to determine the molecular mechanism of the GPI anchor biosynthetic pathway in tumor killing. Deletion of the *PIGP* gene in HAP1 cells abrogated surface expression of GPI-APs (Figs. 2A and 4A and fig. S9A). We mixed the *PIGP* KO cells with wild-type (WT) HAP1 cells and examined their sensitivity to TALL-104–mediated cytotoxicity in a competition assay, which accurately measures the proliferation and death of cell populations (*40*). We observed that the ratio of WT and *PIGP* KO cells did not change significantly during passage in the absence of TALL-104 cells (Fig. 4, A and B), confirming that *PIGP* mutations do not affect cell growth. By contrast, *PIGP* KO cells were strongly enriched after two rounds of TALL-104 treatment (Fig. 4, A and B). These data demonstrate that mutation of the GPI biosynthetic pathway in HAP1 cells causes resistance to TALL-104–mediated killing, validating the result of our genetic screens. Likewise, mutation of *PIGP* in 786-O cells, a human renal cancer cell line (*41*), caused resistance of the cells to TALL-104–mediated killing (Fig. 4C). Thus, the role of the GPI biosynthetic pathway in tumor killing is not limited to HAP1 cells.

TALL-104–mediated killing closely resembles NK cell–mediated cytotoxicity (Figs. 1 and 2) (*42*). Next, we directly examined how *PIGP* KO cells respond to NK cell–mediated cytotoxicity. Using a propidium iodide (PI) uptake assay, we observed that *PIGP* KO cells were substantially more resistant to killing by primary human NK cells (fig. S9B). Thus, mutation of the GPI biosynthetic pathway in target cells also impairs NK cell–mediated cytotoxicity.

We then tested how the GPI biosynthetic pathway regulates tumor surface molecules required for MHC-unrestricted cytotoxicity. Both TRAIL receptor and PVR (Poliovirus receptor) regulate TALL-104–mediated killing (Fig. 2) (*15*, *16*). However, surface levels of these molecules were not reduced in *PIGP* KO cells (Fig. 4D), indicating that their functions are independent of the GPI biosynthetic pathway. We then examined UL16-binding proteins (ULBPs), ligands for the activating NK cell receptor NKG2D (*19*). Since multiple ULBP genes were simultaneously expressed in HAP1 cells (Fig. 4D), ULBPs were not recovered in our screens because of functional redundancy. ULBPs are GPI-APs containing a C-terminal GPI anchor, although a subset of ULBPs also have a transmembrane domain (*43*, *44*). It has been suggested that the GPI anchor and transmembrane domain play redundant roles in ULBP surface localization and activation of NKG2D (*43*). However, we observed that surface expression of ULBPs was completely lost in *PIGP* KO cells (Fig. 4D). Thus, despite the presence of transmembrane domains, the GPI anchor is essential to surface expression of ULBPs.

Next, we examined how the GPI biosynthetic pathway in tumor cells influences the function of CLs after cell-cell interaction. A major route of CL-mediated killing involves the secretion of the cytolytic molecules granzyme and perforin (*7*, *10*, *11*), which occurs when cytolytic granules fuse with the plasma membrane of a CL (*8*, *45*). To measure cytolytic granule secretion, we used a flow cytometry–based

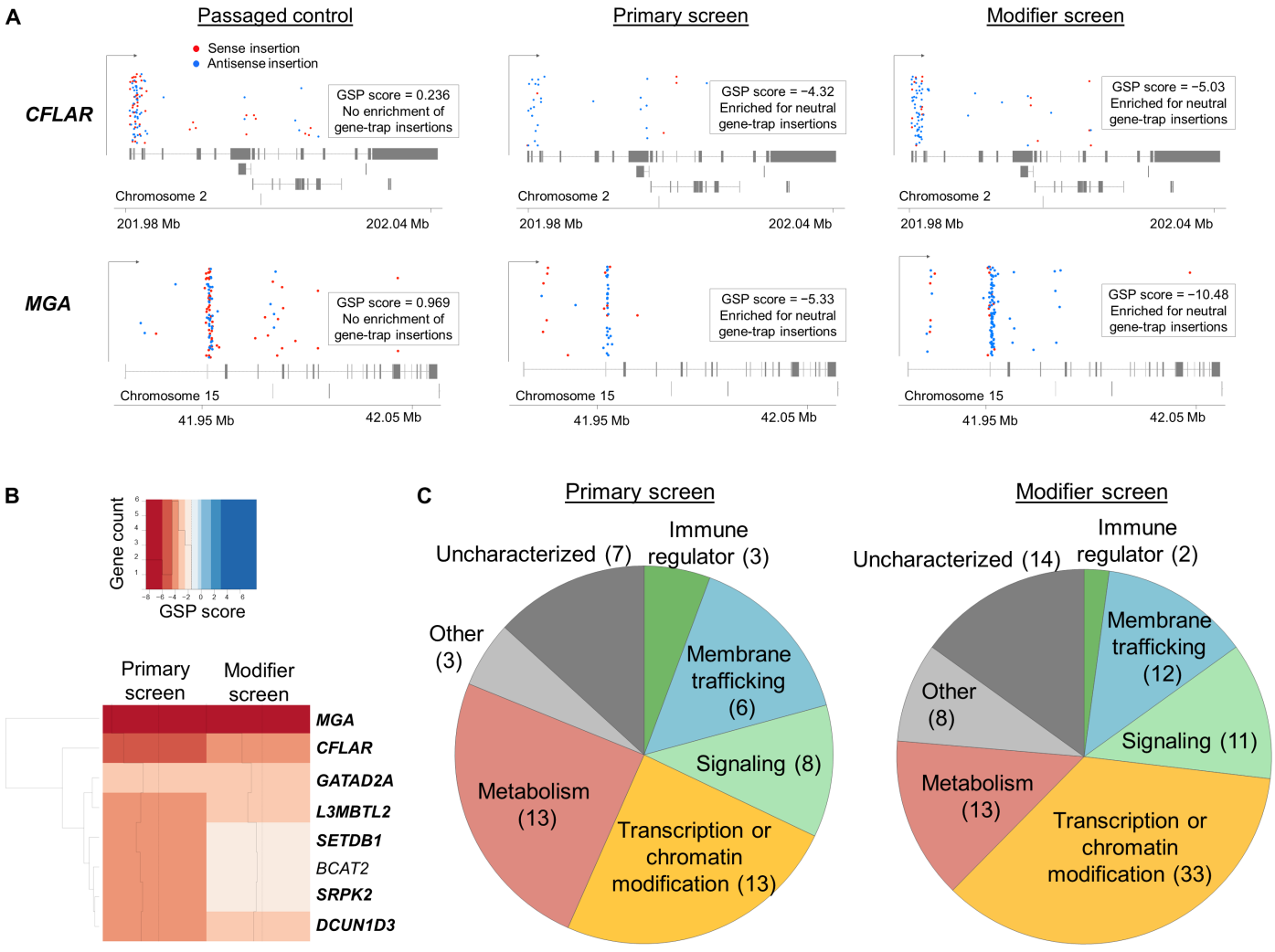

Fig. 3. Identification of negative regulators of TALL-104–mediated tumor killing. (**A**) Visual representations of gene-trap insertions in *CFLAR* and *MGA* in the passage control (no TALL-104 selection), the primary screen, and the modifier screen. The gray boxes indicate exons, while the gray lines indicate introns. The gray arrows depict the directions of transcription. Chromosomal locations of inactivating, sense gene-trap insertions are shown in red, while chromosomal locations of neutral, antisense insertions are shown in blue. GSP is a new scoring metric based on the numbers of unique sense (inactivating) or antisense (neutral) gene-trap insertion within the introns of a candidate gene. GSP = $[\log_2(S/A) \times \log_{10}(S \times A)]$, where "*S*" and "*A*" represent the numbers of sense and antisense gene-trap insertions, respectively. (**B**) Top: Color key of the heatmap. Bottom: Heatmap showing the genes with significantly negative GSP scores in both the primary and modifier screens but not in the passage control. The complete lists of genes are included in fig. S8 and tables S5 and S6. The GSP scores of the genes were quantile-normalized. Genes with significantly negative GSP scores in both screens were clustered using the Euclidean distance metric. Dashed gray lines represent the sample mean, while the solid gray lines represent each hit's GSP score relative to the sample mean. The color of each bar represents the GSP score. Genes associated with cancer or CL killing are highlighted in bold. Cancer association is based on the COSMIC database. (**C**) Summary of the negative regulators identified in the primary and modifier screens based on annotated or predicted gene function. Full datasets are shown in tables S5 and S6.

degranulation assay to quantify surface levels of lysosomal-associated membrane protein 1 (LAMP1; also known as CD107a), a cytolytic granule protein that is exposed to the cell surface after cytolytic granules fuse with the plasma membrane (Fig. 4E) (*45*, *46*). LAMP1 is a specific marker for degranulation as the lysosome-like cytolytic granule is not involved in the trafficking of other cytotoxic molecules such as IFN-γ and death receptor ligands (*47*–*50*). Using this degranulation assay, we observed that TALL-104 cells exhibited little surface LAMP1 expression in the absence of HAP1 cells (Fig. 4E), consistent with a lack of cytolytic granule secretion in unstimulated CLs. Incubation with HAP1 cells, however, strongly increased the surface levels of LAMP1 on TALL-104 cells (Fig. 4E). Notably, *PIGP* KO HAP1 cells induced minimal LAMP1 externalization on TALL-104 cells (Fig. 4E), demonstrating that these mutant cells were defective in triggering the secretion of cytolytic molecules.

Besides cytolytic molecules, death ligands such as TRAIL are also used by CLs to kill tumor cells (*10*, *51*). Our screens recovered TRAIL receptors (*TNFRSF10A* and *TNFRSF10B*) as hits (Fig. 2, B and C). In the absence of target cells, TALL-104 cells exhibited low surface levels of TRAIL (Fig. 4F). Incubation with WT HAP1 cells strongly elevated surface TRAIL on TALL-104 cells, while *PIGP* KO HAP1 cells were largely defective in inducing TRAIL surface expression (Fig. 4F). We also examined IFN-γ, a cytokine released by CLs to promote tumor killing. We observed that similar amounts of IFN-γ

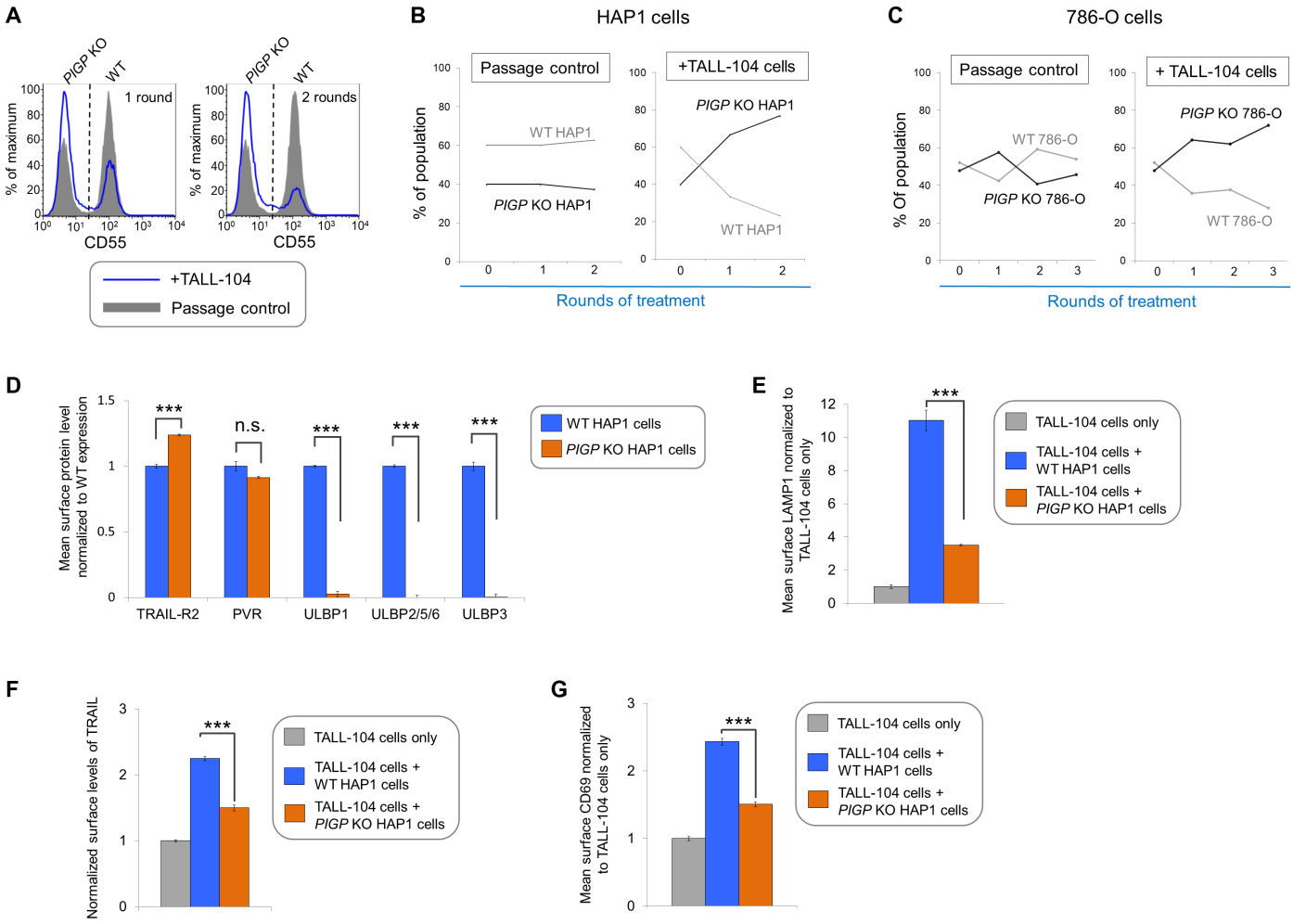

Fig. 4. The GPI biosynthetic pathway is essential to CL activation and cytolytic granule secretion. (**A**) A mixed population of WT and *PIGP* KO HAP1 cells was either untreated or treated with TALL-104 cells. Negative surface staining of CD55, a GPI-AP not involved in CL-mediated killing, was used as a marker for *PIGP* KO cells. $CD55^+$ WT cells and $CD55^-$ *PIGP* KO cells were analyzed by flow cytometry. (**B**) Percentage of WT and *PIGP* KO HAP1 cells in the passage control or TALL-104–treated population. (**C**) Percentage of WT and *PIGP* KO 786-O cells in the passage control or TALL-104–treated population. $CD55^+$ WT cells and $CD55^-$ *PIGP* KO 786-O cells were quantified by flow cytometry after each round of treatment. Data in (B) and (C) are presented as mean values ($n = 3$). (**D**) Normalized surface levels of immune regulators on WT and *PIGP* KO HAP1 cells. (**E**) TALL-104 degranulation presented as normalized surface levels of LAMP1 on TALL-104 cells. (**F**) Normalized surface levels of TRAIL on TALL-104 cells. (**G**) Normalized surface levels of CD69 on TALL-104 cells. Data in (D) to (G) are presented as means ± SD ($n = 3$). *P* values were calculated using Student's *t* test. n.s., $P > 0.05$. ***$P < 0.001$.

were released from NK cells when they were incubated with WT or *PIGP* KO HAP1 cells (fig. S10). Thus, IFN-γ release is not dependent on the GPI biosynthetic pathway of tumor cells.

We then determined whether the GPI biosynthetic pathway regulates CL activation. We examined the surface expression of CD69, an activation marker of NK cells (*52*, *53*). We observed that TALL-104 cells displayed low surface CD69 expression in the absence of HAP1 cells (Fig. 4G). Addition of WT HAP1 cells strongly elevated surface levels of CD69 on TALL-104 cells (Fig. 4G). By contrast, *PIGP* KO HAP1 cells were largely defective in inducing CD69 expression (Fig. 4G). Thus, *PIGP* is essential to the activation of TALL-104 cells by tumor cells, consistent with its roles in cytolytic granule secretion and TRAIL expression. Together, these data indicate that the GPI biosynthetic pathway of tumor cells is required for the activation and cytotoxic functions of MHC-unrestricted CLs, providing a molecular explanation for its activating role in MHC-unrestricted cytotoxicity.

PBRM1 regulates ULBP expression in target cells and promotes cytolytic granule secretion in MHC-unrestricted CLs

We next characterized PBRM1, a subunit of the PBAF chromatin-remodeling complex mutated in a large number of human cancers (Figs. 2 and 5A) (*31*, *32*, *54*). To validate the functional role of PBRM1 in TALL-104–mediated cytotoxicity, we deleted the *PBRM1* gene in HAP1 cells using CRISPR-Cas9 (Fig. 5B). WT and *PBRM1* KO HAP1 cells were mixed and subjected to multiple rounds of TALL-104 treatment in a competition assay. We observed that *PBRM1* KO cells were significantly enriched after three rounds of TALL-104 treatment (Fig. 5, C and D). By contrast, the ratio of WT and *PBRM1* KO cells did not change significantly during passage in the absence of TALL-104 selection (Fig. 5, C and D), confirming that *PBRM1* KO did not affect cell growth (*32*, *55*). These results demonstrate that deletion of the *PBRM1* gene in target cells caused resistance to TALL-104–mediated killing, validating the finding of

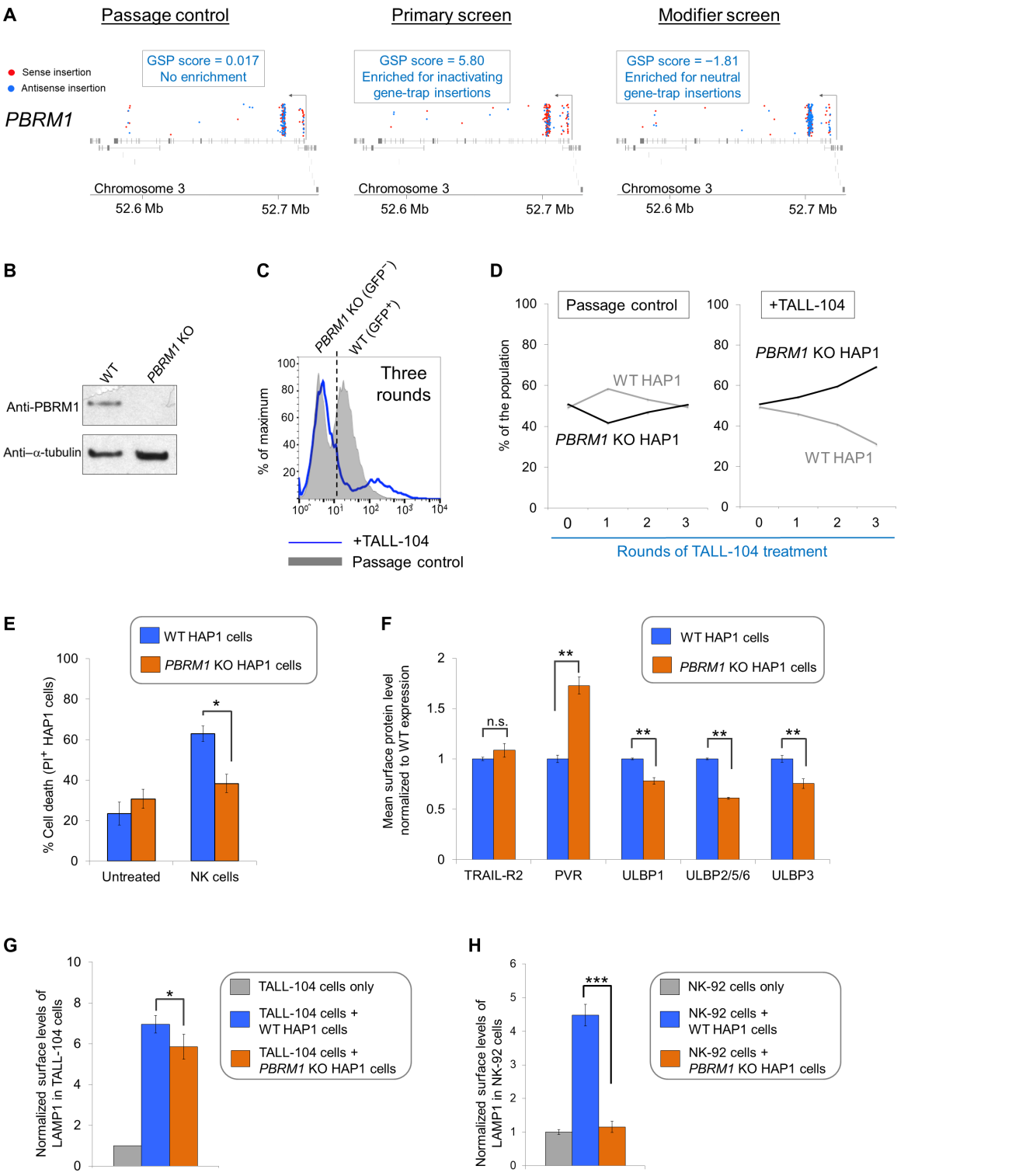

Fig. 5. PBRM1 regulates ULBP expression in target cells and promotes cytolytic granule secretion in CLs. (**A**) Visual representations of gene-trap insertions in the *PBRM1* gene in the screens. The gray boxes indicate exons, and the gray lines indicate introns. The gray arrows depict the direction of transcription. (**B**) Immunoblot showing PBRM1 expression in WT HAP1 cells and a clonal *PBRM1* KO HAP1 cell line. *PBRM1* mRNA expression in these cells is shown in fig. S13. (**C**) WT (GFP^+) and *PBRM1* KO (GFP^-) cells in mixed populations were quantified by flow cytometry after three rounds of passage or TALL-104 treatment. (**D**) Percentage of WT and *PBRM1* KO HAP1 cells in the passage control or TALL-104–treated population. Data are presented as mean values ($n = 3$). (**E**) Percentage of propidium iodide–positive WT and *PBRM1* KO HAP1 cells after treatment with primary human NK cells. (**F**) Mean surface levels of immune regulators on WT and *PBRM1* KO HAP1 cells. (**G**) TALL-104 degranulation presented as normalized surface levels of LAMP1 on TALL-104 cells after incubation with target cells. (**H**) NK-92 degranulation presented as normalized surface levels of LAMP1 in NK-92 cells. Data in (E) to (H) are presented as means ± SD ($n = 3$). *P* values were calculated using Student's *t* test. n.s., $P > 0.05$. $^*P < 0.05$, $^{**}P < 0.01$, $^{***}P < 0.001$.

our genetic screen. Next, we examined the sensitivity of the cells to primary human NK cells. While WT HAP1 cells were efficiently killed by NK cells, *PBRM1* KO cells were substantially more resistant to killing (Fig. 5E), confirming the critical role of PBRM1 in NK cell–mediated cytotoxicity.

Next, we further examined how PBRM1 regulates the response of tumor cells to killing. Since loss of MHC class I promotes killing by MHC-unrestricted CLs (*19*), the resistance of *PBRM1* KO cells to killing could be due to up-regulation of MHC class I. However, we observed that surface levels of MHC class I molecules were moderately reduced in *PBRM1* KO cells (fig. S11), indicating that the resistance of the KO cells to killing was not caused by up-regulation of MHC class I. Surface levels of TRAIL receptor and PVR were not significantly reduced in the KO cells (Fig. 5F). Mutation of *PBRM1* markedly decreased surface expression of ULBPs in HAP1 cells (Fig. 5F). Thus, like PIGP, PBRM1 broadly regulates surface expression of ULBPs in target cells. The overall similarity of *PIGP* and *PBRM1* KO phenotypes prompted us to examine whether PBRM1 regulates cytolytic granule secretion. Using the flow cytometry–based degranulation assay, we observed that HAP1-triggered externalization of LAMP1 in TALL-104 cells was markedly reduced when *PBRM1* was mutated (Fig. 5G). Likewise, KO of *PBRM1* diminished the ability of HAP1 cells to induce LAMP1 externalization in NK cells (Fig. 5H). Thus, PBRM1 is required for triggering cytolytic granule secretion from MHC-unrestricted CLs. We also tested other molecules of CLs involved in target cell killing. We observed that target cell–induced surface expression of TRAIL in TALL-104 cells was reduced when *PBRM1* was mutated in HAP1 cells (fig. S12). By contrast, target cell–induced IFN-γ release was not affected by *PBRM1* KO in HAP1 cells (fig. S10). Together, these results demonstrate that PBRM1 regulates ULBP expression in tumor cells and promotes cytolytic granule secretion from MHC-unrestricted CLs.

DISCUSSION

This work revealed a complex network of tumor-intrinsic factors that positively or negatively regulate the response of tumor cells to NK cells and other clinically significant MHC-unrestricted CLs. Mutations of these factors either cause resistance or enhance sensitivity to killing. The screens identified known genes involved in NK cell–mediated killing such as ligands of NK cell receptors. Most of the genes isolated in the screens, however, were not previously linked to tumor killing. Notably, most of our hits including PBRM1 and GPI biosynthetic genes were not recovered in previous attempts to genetically dissect NK cell–mediated killing (*56*–*58*), likely because of the unique genetic screening platform used in this work. The advantages of this platform include homogeneous populations of CLs with consistent tumor-killing activities and a multiround selection procedure that can identify genes with a wide range of KO phenotypes.

A large portion of the genes identified in the screens were mutated in human cancers. Most of these genes do not regulate cell proliferation or response to T cell–mediated cytotoxicity, suggesting that their mutations promote cancer progression by impairing NK cell–mediated killing of tumor cells. These findings will be valuable for personalized evaluation of cancer genomes and immunotherapeutic strategies. An unexpected discovery of this study is that the genes regulating tumor response to killing are fundamentally distinct between MHC-unrestricted and MHC-restricted CLs. While a subset of our hits including the IFN-γ receptor and CFLAR are also involved in T cell–mediated killing (*33*–*35*), the vast majority of the genes identified in our screens are unique to tumor response to MHC-unrestricted cytotoxicity. Likewise, most of the genes identified in previous T cell–based screens were not involved in tumor response to killing by MHC-unrestricted CLs. Knowledge of tumor responses to MHC-unrestricted CLs is integral to understanding how tumor cells interact with the immune system and how they evade cancer immunosurveillance to develop into metastatic malignancies.

A major group of genes identified in our screens encode enzymes involved in the biosynthesis of the GPI anchor. We found that mutation of GPI biosynthetic pathway abolishes the surface expression of all ULBPs. This finding indicates that, although certain ULBPs also have transmembrane domains besides the GPI anchor, the GPI anchor is essential for their surface localization. Thus, manipulation of the GPI biosynthetic pathway has the potential to simultaneously target the entire ULBP family of proteins. It is possible that ULBP deficiency fully accounts for the defects of activation and cytotoxic functions of CLs caused by mutations of GPI biosynthesis. However, since cells express nearly 200 GPI-APs (*59*), it remains possible that additional GPI-APs other than ULBPs are also involved in tumor cells' response to killing.

An unexpected finding of this study is that PBRM1 plays opposite roles in MHC-restricted and MHC-unrestricted tumor killing. A tumor suppressor mutated in a number of tumors including clear-cell renal cell carcinoma (*31*, *32*, *35*, *54*), PBRM1 negatively regulates T cell–mediated tumor killing by modulating the expression of cytotoxic signaling molecules (*32*, *35*). While this inhibitory activity correlates well with the clinical benefits of *PBRM1* mutations in checkpoint therapies (*32*, *35*), it cannot fully explain the tumor suppressor role of PBRM1. Our findings suggest that *PBRM1* mutations promote tumorigenesis by impairing NK cell–mediated clearance of tumor cells. PBRM1 regulates surface expression of ULBPs, which are NKG2D ligands. The overall KO phenotype of *PBRM1* is remarkably similar to that of *PIGP*, suggesting that *PBRM1* may control the expression, maturation, or localization of a GPI biosynthetic gene(s) rather than individual ULBPs. Further research using human samples and mouse models will be needed to test this possibility.

Both the innate and adaptive immune systems are involved in cancer immunosurveillance, and cancer arises when both systems fail (*7*, *12*). Given the complementary nature of MHC-restricted and MHC-unrestricted CLs in tumor killing, it is conceivable that combinatorial therapies using both types of CLs would achieve the best therapeutic outcomes. NK cells are capable of detecting and eliminating tumor cells refractory to T cell–mediated cytotoxicity and are particularly powerful in eradicating metastatic tumor cells and cancer stem cells (*11*–*13*). To be effective, cancer immunotherapies must overcome resistance to CL-mediated cytotoxicity. The large number of tumor-intrinsic factors identified in this work provides a rich source of potential targets to enhance and maintain the response of tumor cells to endogenous NK cells or engineered NK cells and NK-like cell lines in adoptive transfer therapies.

MATERIALS AND METHODS

Cell culture and reagents

HAP1 cells were cultured in Iscove's Modified Dulbecco's Medium (IMDM) supplemented with 10% fetal bovine serum (FBS), L-glutamine, and penicillin/streptomycin. 293T cells were cultured in Dulbecco's modified Eagle's medium (DMEM) supplemented with 20% FBS,

L-glutamine, and penicillin/streptomycin. 786-O cells [American Type Culture Collection (ATCC), no. CRL-1932] were cultured in RPMI 1640 supplemented with 10% FBS, L-glutamine, and penicillin/streptomycin. NK-92 cells (ATCC, no. CRL-2407) were cultured in minimum essential medium Eagle, alpha modification supplemented with 12.5% FBS, 12.5% Donor Equine Serum, 2 mM L-glutamine, 0.2 mM myo-inositol (Acros Organics, no. 122261000), 0.1 mM 2-mercaptoethanol, 0.02 mM folic acid (Acros Organics, no. 216630100), and recombinant human interleukin-1 (IL-2) (100 U/ml) (PeproTech, no. 200-02). TALL-104 cells (ATCC, no. CRL-11386) were cultured in IMDM supplemented with 20% FBS, human albumin (2.5 μg/ml) (Sigma-Aldrich, no. A9731), D-mannitol (0.5 μg/ml) (Acros Organics, no. 125345000), and recombinant human IL-2 (100 U/ml). Primary NK cells (ZenBio, no. SER-PBCD56 + NK-F) were cultured in RPMI 1640 supplemented with 10% FBS, L-glutamine, penicillin/streptomycin, sodium pyruvate, MEM nonessential amino acids, recombinant human IL-2 (100 U/ml), and recombinant human IL-15 (10 U/ml) (PeproTech, no. 200-15). PBMCs (ZenBio, no. SER-PBMC-200) were cultured in RPMI 1640 supplemented with 10% FBS, L-glutamine, penicillin/streptomycin, sodium pyruvate, and MEM nonessential amino acids. Human ASCs (ZenBio, no. ASC-F) were grown in DMEM/Ham's F-12 (1:1) media supplemented with 10% FBS and penicillin/streptomycin.

Generation of mutant HAP1 cell libraries

Mutant HAP1 libraries were produced using a previously described procedure (*28*). Briefly, gene-trap retroviruses were generated by transfecting six T175 flasks of 293T cells with a cocktail of plasmids including pGT-GFP0, pGT-GFP1, pGT-GFP2, pAdVAntage (Promega, no. E1711), pGAL, and pCMV-VSVG using TurboFectin 8.0 (OriGene, no. TF81001). The retroviruses were collected 40 hours after transfection, and again 50 hours after transfection. The retroviruses were concentrated in a Beckman SW 28 rotor at 25,000 rpm for 1.5 hours. Viral pellets were resuspended in 500 μl of phosphate-buffered saline (PBS) overnight at 4°C. HAP1 cells (1.5×10^8) were spin-infected twice at 12-hour intervals with 1.5× viral concentrate (by flask surface area) in the presence of protamine sulfate (8 μg/ml). After mixture with virus, cells were plated in 12-well plates at 1.5×10^6 cells per well and centrifuged at 900*g* for 1.5 hours at room temperature in a Thermo Fisher Scientific Legend RT$^+$ centrifuge. The multiplicity of infection was kept below 1.0 on the basis of green fluorescent protein (GFP) fluorescence. The GPI-deficient library used in the modifier screen was generated using the above protocol. To produce a mutant library in GPI-AP–deficient HAP1 cells, unaltered HAP1 cells were spin-infected with lentiCRISPR virus targeting *PIGP* (see the "Genome editing using CRISPR-Cas9" section). Infected cells were stained for surface CD59 by incubation with anti-CD59 (eBioscience, no. 17-0596) antibodies followed by incubation with allophycocyanin (APC)–conjugated anti-mouse secondary antibodies (eBioscience, no. 17-4015) (see the "Flow cytometry measurements" section). HAP1 cells with low cell size (forward scatter) and lack of surface CD59 protein (APC) were collected by fluorescence-activated cell sorting (MoFlo, Beckman Coulter) to isolate a haploid GPI-AP deficient population. This population was used to produce an additional gene-trap library as described above.

Genome-wide haploid genetic dissection of TALL-104–mediated tumor killing

A HAP1 cell library consisting of ~1.5×10^8 mutagenized cells was thawed and allowed to recover for 3 days. The cells were plated at a density of 5×10^6 cells per 100-mm plate. One population of 1.5×10^8 cells was plated for selection, and another population of 1.5×10^8 cells was plated for passage throughout the duration of the screen. HAP1 cells were incubated with approximately equal numbers of TALL-104 cells in the presence of IL-2 (100 U/ml) and the following inhibitor cocktail: soluble TRAIL-R2-Fc chimera at a final concentration of 20 ng/ml (R&D Systems, no. 631-T2-100), soluble TNFR1p55 at a final concentration of 100 ng/ml (a gift of C. Edwards, University of Colorado School of Medicine), soluble tumor necrosis factor receptor 1 (TNFR1)–Fc at a final concentration of 5 ng/ml (R&D Systems, no. 372-RI-050), soluble Fas-Fc chimera at a final concentration of 100 ng/ml (R&D Systems, no. 326-FS-050), and LEAF purified anti-human Fas-L at a final concentration of 50 ng/ml (BioLegend, no. 306409). This inhibitor cocktail was intended to partially inhibit the fast-acting death-receptor killing pathways such that the slower granzyme/perforin cytotoxic pathway could also be reflected in the screen.

The killing and detachment of HAP1 cells were periodically examined until ~50% of the HAP1 cells detached from the plate, which usually took 8 to 12 hours. After treatment, the HAP1 cells were washed once with PBS to remove free TALL-104 cells, and fresh media were added. After 24 hours, the HAP1 cells were dissociated using Accutase (Innovative Cell Technologies, #AT 104), counted, and replated at ~5×10^6 cells per 100-mm plate for the next round of TALL-104 treatment on the following day. The untreated control cells were split, counted, and replated at a similar total cell number and density as the TALL-104–treated HAP1 population. After four rounds of TALL-104 treatment, HAP1 cells were expanded and 5×10^7 cells were used for genomic DNA extraction and linear polymerase chain reaction (PCR) reactions. The modifier screen using *PIGP* KO HAP1 cells was completed using a similar protocol as the primary screen, except that HAP1 cells were plated at a density of ~4×10^6 cells per 100-mm plate and the ratio of TALL-104 to HAP1 cells was approximately 2:1 during treatment.

Deep sequencing of retroviral gene-trap insertions

Genomic DNA was extracted from HAP1 cells using a genomic DNA purification kit (Thermo Fisher Scientific, no. K0721). Linear PCR was performed using 2 μg of genomic DNA as template and the following primer: [5′-Biotin-GGTCTCCAAATCTCGGTGGAAC-3′]. After 125 cycles of amplification, the linear PCR products were purified using biotin-binding Dynabeads (Thermo Fisher Scientific, no. 11047). On-bead ligation of a 5′phosphorylated, 3′-ddC linker was performed using CircLigase II (Epicentre, no. CL9021K). The product was purified and used as a template for PCR to add Illumina adapter sequences I (5′-AATGATACGGCGACCACCGAGATCTGATGGTTCTCTAGCTTGCC-3′) and II (5′-CAAGCAGAAGACGGCATACGA-3′). PCR products from 8 to 30 individual PCR reactions were extracted from a 1% tris-acetate-EDTA–agarose gel, pooled over a Qiagen Spin column (Qiagen, no. 28706), and sequenced in a lane of the Illumina HiSeq 2000 using a custom primer recognizing the 5′end of the LTR (5′-CTAGCTTGCCAAACCTACAGGTGGGGTCTTTCA-3′).

Bioinformatic analysis of retroviral gene-trap insertions

FASTQ files from Illumina sequencing were preprocessed to filter duplicate reads using custom scripts. FASTQ files containing unique sequences were aligned to the human genome (hg19) using the Bowtie software v0.12.08 (*60*). The 50–base pair (bp) FASTQ

sequences were trimmed from their 3′ ends to a length of 35 bp, and were aligned in "—best mode" allowing one mismatch. Reads with more than one genomic alignment were suppressed. Aligned sequences were intersected with gene tables obtained from the University of California, Santa Cruz Genome Browser (hg19) containing either exons or introns using BEDTools software v2.17.0 (*61*). Unique insertions per gene were counted for exons and for introns. The total numbers of unique sense and antisense insertions within introns were counted for each gene. Fisher's exact test was calculated using previously published passage control data (*28*, *62*). We developed custom scripts in Python using NumPy, Pandas, SciPy, and matplotlib modules for downstream data analysis, statistics, and visualization. Heatmaps were generated by normalizing unique insertion counts per gene using the quantile method in R. Normalized values were used as input for heatmap.2 (package "gplots") run in R. Insertion plots were produced using the package "Gviz" in R (www.r-project.org/). GSEA was performed using GSEA from the Broad Institute (*36*).

Genome editing using CRISPR-Cas9

Guide sequences were designed according to previously published protocols (*63*). Double-stranded oligonucleotides containing the guide sequences were individually subcloned into pLentiCRISPR V2-puro vectors as previously described (*28*, *64*). The *PIGP* gene was mutated using one guide, while the *PBRM1* gene was mutated by simultaneous introduction of two independent guide sequences. The following guide sequences were used in this study. The protospacer adjacent motifs are underlined: *PIGP*: 5′-TACAGTACTTTACCTCGTGTGGG-3′; *PBRM1* exon 1: 5′-GAAACCACTTCATAATAGTCTGG-3′; *PBRM1* exon 4: 5′-TTGCAAGCGGCTTTATATTCAGG-3′.

Flow cytometry measurements

Adherent cells were detached from culture plates using Accutase to preserve surface antigens for flow cytometry measurements (*64*–*66*). Cells were labeled using the indicated mouse monoclonal primary antibodies and APC-conjugated anti-mouse secondary antibodies (eBioscience, no. 17-4015) or Alexa Fluor 488–conjugated anti-mouse immunoglobulin G2a secondary antibodies (Invitrogen, #A-21131). Exceptions were phycoerythrin (PE)–conjugated anti-CD55 antibodies (eBioscience, no. 12-0559-42), APC-conjugated anti-CD45 antibodies (eBioscience, no. 17-0459-42), APC-conjugated anti–HLA-A/B/C antibodies (BioLegend, no. 311409), APC-conjugated anti–β2-microglobulin antibodies (BioLegend, no. 395711), and eFluor 450–conjugated anti-CD69 antibodies (eBioscience, no. 48-0699-41). The following unconjugated primary antibodies were used in this study: anti-CD3 antibodies (eBioscience, no. 14-0038-82), anti-CD56 antibodies (eBioscience, no. 14-0567-82), anti-CD314/NKG2D antibodies (BioLegend, no. 320802), anti-CD337/NKp30 antibodies (BioLegend, no. 325202), anti-PrP antibodies (eBioscience, no. 14-9230), anti-CD59 antibodies (eBioscience, no. 17-0596), anti-CD261/TRAIL-R1 antibodies (eBioscience, no. 14-6644-80), anti-CD262/TRAIL-R2 antibodies (eBioscience, no. 14-9909-82), anti-CD155/PVR antibodies (BioLegend, no. 337602), anti-ULBP1 antibodies (R&D Systems, no. MAB1380), anti-ULBP2/5/6 antibodies (R&D Systems, no. MAB1298), anti-ULBP3 antibodies (R&D Systems, no. MAB1517), anti-LAMP1/CD107a antibodies (eBioscience, no. 14-1079-80), and anti-CD253/TRAIL antibodies (eBioscience, no. 16-9927-82). Flow cytometry data were collected on the CyAn ADP Analyzer (Beckman Coulter). Data from populations of approximately 10,000 cells were analyzed using FlowJo 10.1. All flow cytometry experiments were run in biological triplicate to calculate statistical significance.

Immunoblotting

Cells were lysed in an SDS sample buffer, and the samples were resolved on 8% bis-tris SDS–polyacrylamide gel electrophoresis. PIGP and PBRM1 were detected using rabbit polyclonal anti-PIGP antibodies (Sino Biological, #204171-T36) and rabbit polyclonal anti-PBRM1/BAF180 antibodies (Bethyl Laboratories, no. A301-591A-T), respectively, and horseradish peroxidase–conjugated anti-rabbit secondary antibodies (Sigma-Aldrich, no. A6154). α-Tubulin was probed using mouse monoclonal anti–α-tubulin antibodies (eBioscience, no. 14-4502-82) and horseradish peroxidase–conjugated anti-mouse secondary antibodies (Sigma-Aldrich, no. A6782).

TALL-104–mediated killing assay

WT and mutant target cells were mixed at a 1:1 ratio and plated in six-well plates in six replicates at a density of 3.5×10^5 cells per well. After 24 hours, TALL-104 cells were added to three replicates of target cells at a 1:1 ratio. An additional three replicates were passage controls. After 8 hours, the TALL-104 cells were removed by aspiration and washing with PBS. Target cells attached to the plates were allowed to recover overnight. Subsequently, target cells were collected using Accutase digestion. Approximately half of the collected target cells were plated for an additional round of TALL-104 treatment, while the remaining cells were prepared for flow cytometry measurements. Flow cytometry was used to measure the ratio of WT to mutant target cells in each population.

Primary NK cell–mediated killing assay

Target cells were plated at ~10^5 cells per well in a 24-well plate. After 24 hours, primary human NK cells were stained with APC-conjugated anti-CD45 antibodies and added to target cells at a 1:1 ratio in the presence of IL-2, IL-15, and the inhibitor cocktail. After incubation, both nonadherent and adherent cells were collected using Accutase digestion. The cells were stained with propidium iodide and assayed by flow cytometry.

CL degranulation assay

Target cells were plated at ~10^5 cells per well in a 24-well plate. After 24 hours, CLs (TALL-104 or NK cells) were added to the target cells at a 1:1 ratio in the presence of IL-2 and the inhibitor cocktail. After incubation for 4 hours, both nonadherent and adherent cells were collected using Accutase digestion. The cells were stained with anti-LAMP1 antibodies (eBioscience, no. 14-1079-80) and PE-conjugated anti-mouse secondary antibodies (BioLegend, no. 406608), as well as APC-conjugated anti-CD45 antibodies (eBioscience, no. 17-0459-42). Only $CD45^+$ CLs were included in the analysis (target cells were $CD45^-$). CL degranulation was quantified as the fold change of mean LAMP1 protein surface staining normalized to a CL-only control.

Measurement of TRAIL surface levels on CLs

Target cells were plated at ~10^5 cells per well in a 24-well plate. After 24 hours, CLs (TALL-104 or NK cells) were added to the target cells at a 1:1 ratio in the presence of IL-2. After incubation for 24 hours, both nonadherent and adherent cells were collected using Accutase digestion. The cells were stained with anti-CD253/TRAIL antibodies (eBioscience, no. 16-9927-82), PE-conjugated anti-mouse secondary

antibodies, and APC-conjugated anti-CD45 antibodies. TRAIL surface levels on $CD45^+$ CLs were quantified using flow cytometry.

Measurement of the CL activation marker CD69

Target cells were plated at ~10^5 cells per well in a 24-well plate. After 24 hours, CLs were added to the target cells at a 1:1 ratio in the presence of IL-2 and the inhibitor cocktail. After incubation for 48 hours, both nonadherent and adherent cells were collected using Accutase digestion. The cells were stained with eFluor 450–conjugated anti-CD69 antibodies (eBioscience, no. 48-0699-41) and APC-conjugated anti-CD45 antibodies. Surface levels of CD69 in $CD45^+$ CLs were quantified using flow cytometry.

Real-time quantitative reverse transcription PCR

Total RNAs were isolated using the RNeasy Mini Kit (Qiagen, no. 74104), followed by treatment with ezDNAse (Thermo Fisher Scientific, no. 18091150). First strand complementary DNA synthesis was performed using a SuperScript IV kit (Thermo Fisher Scientific, no. 18091050). Gene expression was determined by quantitative reverse transcription PCR on a Bio-Rad CFX384 Real-time PCR Detection System using SsoAdvanced Universal SYBR Green Supermix (Bio-Rad, no. 172-5272) with gene-specific primer sets. The cycle threshold values of a candidate gene were normalized to those of *GAPDH*, a reference gene, and the Δcycle threshold values were calculated. The results were plotted as fold changes relative to the WT sample.

PCR primers for *PBRM1* were as follows: CGGGTGTGATGAACCAAGGA (forward) and

TTGGCTGCTGTATGACAGGG (reverse). PCR primers for *GAPDH* were as follows: GACAGTCAGCCGCATCTTCT (forward) and GCGCCCAATACGACCAAATC (reverse).

SUPPLEMENTARY MATERIALS

Supplementary material for this article is available at http://advances.sciencemag.org/cgi/content/full/6/48/eabc3243/DC1

View/request a protocol for this paper from *Bio-protocol*.

REFERENCES AND NOTES

1. Q. Hammer, T. Rückert, C. Romagnani, Natural killer cell specificity for viral infections. *Nat. Immunol.* **19**, 800–808 (2018).
2. P. Sharma, S. Hu-Lieskovan, J. A. Wargo, A. Ribas, Primary, adaptive, and acquired resistance to cancer immunotherapy. *Cell* **168**, 707–723 (2017).
3. D. S. Chen, I. Mellman, Elements of cancer immunity and the cancer-immune set point. *Nature* **541**, 321–330 (2017).
4. T. K. Kim, R. S. Herbst, L. Chen, Defining and understanding adaptive resistance in cancer immunotherapy. *Trends Immunol.* **39**, 624–631 (2018).
5. P. Sharma, J. P. Allison, Immune checkpoint targeting in cancer therapy: Toward combination strategies with curative potential. *Cell* **161**, 205–214 (2015).
6. J. H. Russell, T. J. Ley, Lymphocyte-mediated cytotoxicity. *Annu. Rev. Immunol.* **20**, 323–370 (2002).
7. M. Barry, R. C. Bleackley, Cytotoxic T lymphocytes: All roads lead to death. *Nat. Rev. Immunol.* **2**, 401–409 (2002).
8. J. Lieberman, The ABCs of granule-mediated cytotoxicity: New weapons in the arsenal. *Nat. Rev. Immunol.* **3**, 361–370 (2003).
9. A. H. Sharpe, K. E. Pauken, The diverse functions of the PD1 inhibitory pathway. *Nat. Rev. Immunol.* **18**, 153–167 (2018).
10. E. O. Long, H. S. Kim, D. Liu, M. E. Peterson, S. Rajagopalan, Controlling natural killer cell responses: Integration of signals for activation and inhibition. *Annu. Rev. Immunol.* **31**, 227–258 (2013).
11. C. I. Dahlberg, D. Sarhan, M. Chrobok, A. D. Duru, E. Alici, Natural killer cell-based therapies targeting cancer: Possible strategies to gain and sustain anti-tumor activity. *Front. Immunol.* **6**, 605 (2015).
12. C. Guillerey, N. D. Huntington, M. J. Smyth, Targeting natural killer cells in cancer immunotherapy. *Nat. Immunol.* **17**, 1025–1036 (2016).
13. J. Koch, A. Steinle, C. Watzl, O. Mandelboim, Activating natural cytotoxicity receptors of natural killer cells in cancer and infection. *Trends Immunol.* **34**, 182–191 (2013).
14. C. A. Kruse, S. Visonneau, B. K. Kleinschmidt-DeMasters, C. J. Gup, G. G. Gomez, D. B. Paul, D. Santoli, The human leukemic T-cell line, TALL-104, is cytotoxic to human malignant brain tumors and traffics through brain tissue: Implications for local adoptive immunotherapy. *Cancer Res.* **60**, 5731–5739 (2000).
15. M. Daher, K. Rezvani, Next generation natural killer cells for cancer immunotherapy: The promise of genetic engineering. *Curr. Opin. Immunol.* **51**, 146–153 (2018).
16. K. Rezvani, R. Rouce, E. Liu, E. Shpall, Engineering natural killer cells for cancer immunotherapy. *Mol. Ther.* **25**, 1769–1781 (2017).
17. O. Demaria, S. Cornen, M. Daëron, Y. Morel, R. Medzhitov, E. Vivier, Harnessing innate immunity in cancer therapy. *Nature* **574**, 45–56 (2019).
18. S. Visonneau, A. Cesano, D. L. Porter, S. L. Luger, L. Schuchter, M. Kamoun, M. H. Torosian, K. Duffy, C. Sickles, E. A. Stadtmauer, D. Santoli, Phase I trial of TALL-104 cells in patients with refractory metastatic breast cancer. *Clin. Cancer Res.* **6**, 1744–1754 (2000).
19. M. G. Morvan, L. L. Lanier, NK cells and cancer: You can teach innate cells new tricks. *Nat. Rev. Cancer* **16**, 7–19 (2016).
20. H. Klingemann, L. Boissel, F. Toneguzzo, Natural killer cells for immunotherapy–advantages of the NK-92 cell line over blood NK cells. *Front. Immunol.* **7**, 91 (2016).
21. C. Brando, S. Mukhopadhyay, E. Kovacs, R. Medina, P. Patel, T. L. Catina, K. S. Campbell, D. Santoli, Receptors and lytic mediators regulating anti-tumor activity by the leukemic killer T cell line TALL-104. *J. Leukoc. Biol.* **78**, 359–371 (2005).
22. B. Geoerger, C.-B. Tang, A. Cesano, S. Visonneau, S. Marwaha, K. D. Judy, L. N. Sutton, D. Santoli, P. C. Phillips, Antitumor activity of a human cytotoxic T-cell line (TALL-104) in brain tumor xenografts. *Neuro Oncol.* **2**, 103–113 (2000).
23. G. G. Gomez, S. B. Read, L. E. Gerschenson, D. Santoli, A. Zweifach, C. A. Kruse, Interactions of the allogeneic effector leukemic T cell line, TALL-104, with human malignant brain tumors. *Neuro Oncol.* **6**, 83–95 (2004).
24. T. A. Lyubchenko, G. A. Wurth, A. Zweifach, Role of calcium influx in cytotoxic T lymphocyte lytic granule exocytosis during target cell killing. *Immunity* **15**, 847–859 (2001).
25. J. E. Carette, M. Raaben, A. C. Wong, A. S. Herbert, G. Obernosterer, N. Mulherkar, A. I. Kuehne, P. J. Kranzusch, A. M. Griffin, G. Ruthel, P. Dal Cin, J. M. Dye, S. P. Whelan, K. Chandran, T. R. Brummelkamp, Ebola virus entry requires the cholesterol transporter Niemann-Pick C1. *Nature* **477**, 340–343 (2011).
26. V. A. Blomen, P. Májek, L. T. Jae, J. W. Bigenzahn, J. Nieuwenhuis, J. Staring, R. Sacco, F. R. van Diemen, N. Olk, A. Stukalov, C. Marceau, H. Janssen, J. E. Carette, K. L. Bennett, J. Colinge, G. Superti-Furga, T. R. Brummelkamp, Gene essentiality and synthetic lethality in haploid human cells. *Science* **350**, 1092–1096 (2015).
27. J. E. Carette, C. P. Guimaraes, M. Varadarajan, A. S. Park, I. Wuethrich, A. Godarova, M. Kotecki, B. H. Cochran, E. Spooner, H. L. Ploegh, T. R. Brummelkamp, Haploid genetic screens in human cells identify host factors used by pathogens. *Science* **326**, 1231–1235 (2009).
28. E. M. Davis, J. Kim, B. L. Menasche, J. Sheppard, X. Liu, A.-C. Tan, J. Shen, Comparative haploid genetic screens reveal divergent pathways in the biogenesis and trafficking of glycophosphatidylinositol-anchored proteins. *Cell Rep.* **11**, 1727–1736 (2015).
29. R. Mezzadra, C. Sun, L. T. Jae, R. Gomez-Eerland, E. de Vries, W. Wu, M. E. W. Logtenberg, M. Slagter, E. A. Rozeman, I. Hofland, A. Broeks, H. M. Horlings, L. F. A. Wessels, C. U. Blank, Y. Xiao, A. J. R. Heck, J. Borst, T. R. Brummelkamp, T. N. M. Schumacher, Identification of CMTM6 and CMTM4 as PD-L1 protein regulators. *Nature* **549**, 106–110 (2017).
30. C. S. Brandt, M. Baratin, E. C. Yi, J. Kennedy, Z. Gao, B. Fox, B. Haldeman, C. D. Ostrander, T. Kaifu, C. Chabannon, A. Moretta, R. West, W. Xu, E. Vivier, S. D. Levin, The B7 family member B7-H6 is a tumor cell ligand for the activating natural killer cell receptor NKp30 in humans. *J. Exp. Med.* **206**, 1495–1503 (2009).
31. I. Varela, P. Tarpey, K. Raine, D. Huang, C. K. Ong, P. Stephens, H. Davies, D. Jones, M.-L. Lin, J. Teague, G. Bignell, A. Butler, J. Cho, G. L. Dalgliesh, D. Galappaththige, C. Greenman, C. Hardy, M. Jia, C. Latimer, K. W. Lau, J. Marshall, S. McLaren, A. Menzies, L. Mudie, L. Stebbings, D. A. Largaespada, L. F. A. Wessels, S. Richard, R. J. Kahnoski, J. Anema, D. A. Tuveson, P. A. Perez-Mancera, V. Mustonen, A. Fischer, D. J. Adams, A. Rust, W. Chan-on, C. Subimerb, K. Dykema, K. Furge, P. J. Campbell, B. T. Teh, M. R. Stratton, P. A. Futreal, Exome sequencing identifies frequent mutation of the SWI/SNF complex gene *PBRM1* in renal carcinoma. *Nature* **469**, 539–542 (2011).
32. D. Miao, C. A. Margolis, W. Gao, M. H. Voss, W. Li, D. J. Martini, C. Norton, D. Bossé, S. M. Wankowicz, D. Cullen, C. Horak, M. Wind-Rotolo, A. Tracy, M. Giannakis, F. S. Hodi, C. G. Drake, M. W. Ball, M. E. Allaf, A. Snyder, M. D. Hellmann, T. Ho, R. J. Motzer, S. Signoretti, W. G. Kaelin Jr., T. K. Choueiri, E. M. Van Allen, Genomic correlates of response to immune checkpoint therapies in clear cell renal cell carcinoma. *Science* **359**, 801–806 (2018).
33. R. T. Manguso, H. W. Pope, M. D. Zimmer, F. D. Brown, K. B. Yates, B. C. Miller, N. B. Collins, K. Bi, M. W. LaFleur, V. R. Juneja, S. A. Weiss, J. Lo, D. E. Fisher, D. Miao, E. Van Allen, D. E. Root, A. H. Sharpe, J. G. Doench, W. N. Haining, *In vivo* CRISPR screening identifies *Ptpn2* as a cancer immunotherapy target. *Nature* **547**, 413–418 (2017).

34. S. J. Patel, N. E. Sanjana, R. J. Kishton, A. Eidizadeh, S. K. Vodnala, M. Cam, J. J. Gartner, L. Jia, S. M. Steinberg, T. N. Yamamoto, A. S. Merchant, G. U. Mehta, A. Chichura, O. Shalem, E. Tran, R. Eil, M. Sukumar, E. P. Guijarro, C.-P. Day, P. Robbins, S. Feldman, G. Merlino, F. Zhang, N. P. Restifo, Identification of essential genes for cancer immunotherapy. *Nature* **548**, 537–542 (2017).
35. D. Pan, A. Kobayashi, P. Jiang, L. Ferrari de Andrade, R. E. Tay, A. M. Luoma, D. Tsoucas, X. Qiu, K. Lim, P. Rao, H. W. Long, G.-C. Yuan, J. Doench, M. Brown, X. S. Liu, K. W. Wucherpfennig, A major chromatin regulator determines resistance of tumor cells to T cell-mediated killing. *Science* **359**, 770–775 (2018).
36. A. Subramanian, P. Tamayo, V. K. Mootha, S. Mukherjee, B. L. Ebert, M. A. Gillette, A. Paulovich, S. L. Pomeroy, T. R. Golub, E. S. Lander, J. P. Mesirov, Gene set enrichment analysis: A knowledge-based approach for interpreting genome-wide expression profiles. *Proc. Natl. Acad. Sci. U.S.A.* **102**, 15545–15550 (2005).
37. T. Wang, K. Birsoy, N. W. Hughes, K. M. Krupczak, Y. Post, J. J. Wei, E. S. Lander, D. M. Sabatini, Identification and characterization of essential genes in the human genome. *Science* **350**, 1096–1101 (2015).
38. A. R. Safa, c-FLIP, a master anti-apoptotic regulator. *Exp. Oncol.* **34**, 176–184 (2012).
39. C. Scaffidi, I. Schmitz, P. H. Krammer, M. E. Peter, The role of c-FLIP in modulation of CD95-induced apoptosis. *J. Biol. Chem.* **274**, 1541–1548 (1999).
40. J. J. M. Eekels, A. O. Pasternak, A. M. Schut, D. Geerts, R. E. Jeeninga, B. Berkhout, A competitive cell growth assay for the detection of subtle effects of gene transduction on cell proliferation. *Gene Ther.* **19**, 1058–1064 (2012).
41. M. A. Thiede, G. J. Strewler, R. A. Nissenson, M. Rosenblatt, G. A. Rodan, Human renal carcinoma expresses two messages encoding a parathyroid hormone-like peptide: Evidence for the alternative splicing of a single-copy gene. *Proc. Natl. Acad. Sci. U.S.A.* **85**, 4605–4609 (1988).
42. J. S. Orange, Formation and function of the lytic NK-cell immunological synapse. *Nat. Rev. Immunol.* **8**, 713–725 (2008).
43. L. Fernandez-Messina, O. Ashiru, S. Agüera-Gonzalez, H. T. Reyburn, M. Valés-Gómez, The human NKG2D ligand ULBP2 can be expressed at the cell surface with or without a GPI anchor and both forms can activate NK cells. *J. Cell Sci.* **124** (Pt 3), 321–327 (2011).
44. B. G. Gowen, B. Chim, C. D. Marceau, T. T. Greene, P. Burr, J. R. Gonzalez, C. R. Hesser, P. A. Dietzen, T. Russell, A. Iannello, L. Coscoy, C. L. Sentman, J. E. Carette, S. A. Muljo, D. H. Raulet, A forward genetic screen reveals novel independent regulators of ULBP1, an activating ligand for natural killer cells. *eLife* **4**, e08474 (2015).
45. E. J. Blott, G. M. Griffiths, Secretory lysosomes. *Nat. Rev. Mol. Cell Biol.* **3**, 122–131 (2002).
46. M. M. Ménager, G. Ménasché, M. Romao, P. Knapnougel, C.-H. Ho, M. Garfa, G. Raposo, J. Feldmann, A. Fischer, G. de Saint Basile, Secretory cytotoxic granule maturation and exocytosis require the effector protein hMunc13-4. *Nat. Immunol.* **8**, 257–267 (2007).
47. E. Reefman, J. G. Kay, S. M. Wood, C. Offenhäuser, D. L. Brown, S. Roy, A. C. Stanley, P. C. Low, A. P. Manderson, J. L. Stow, Cytokine secretion is distinct from secretion of cytotoxic granules in NK cells. *J. Immunol.* **184**, 4852–4862 (2010).
48. J. Feldmann, I. Callebaut, G. Raposo, S. Certain, D. Bacq, C. Dumont, N. Lambert, M. Ouachée-Chardin, G. Chedeville, H. Tamary, V. Minard-Colin, E. Vilmer, S. Blanche, F. Le Deist, A. Fischer, G. de Saint Basile, Munc13-4 is essential for cytolytic granules fusion and is mutated in a form of familial hemophagocytic lymphohistiocytosis (FHL3). *Cell* **115**, 461–473 (2003).
49. A. Dabrazhynetskaya, J. Ma, A. O. Guerreiro-Cacais, Z. Arany, E. Rudd, J.-I. Henter, K. Karre, J. Levitskaya, V. Levitsky, Syntaxin 11 marks a distinct intracellular compartment recruited to the immunological synapse of NK cells to colocalize with cytotoxic granules. *J. Cell. Mol. Med.* **16**, 129–141 (2012).
50. O. D'Orlando, F. Zhao, B. Kasper, Z. Orinska, J. Müller, I. Hermans-Borgmeyer, G. M. Griffiths, U. Zur Stadt, S. Bulfone-Paus, Syntaxin 11 is required for NK and $CD8^+$ T-cell cytotoxicity and neutrophil degranulation. *Eur. J. Immunol.* **43**, 194–208 (2013).
51. M. J. Smyth, K. Takeda, Y. Hayakawa, J. J. Peschon, M. R. M. van den Brink, H. Yagita, Nature's TRAIL—On a path to cancer immunotherapy. *Immunity* **18**, 1–6 (2003).
52. J. Clausen, B. Vergeiner, M. Enk, A. L. Petzer, G. Gastl, E. Gunsilius, Functional significance of the activation-associated receptors CD25 and CD69 on human NK-cells and NK-like T-cells. *Immunobiology* **207**, 85–93 (2003).
53. L. L. Lanier, D. W. Buck, L. Rhodes, A. Ding, E. Evans, C. Barney, J. H. Phillips, Interleukin 2 activation of natural killer cells rapidly induces the expression and phosphorylation of the Leu-23 activation antigen. *J. Exp. Med.* **167**, 1572–1585 (1988).
54. Y. Jiao, T. M. Pawlik, R. A. Anders, F. M. Selaru, M. M. Streppel, D. J. Lucas, N. Niknafs, V. B. Guthrie, A. Maitra, P. Argani, G. J. A. Offerhaus, J. C. Roa, L. R. Roberts, G. J. Gores, I. Popescu, S. T. Alexandrescu, S. Dima, M. Fassan, M. Simbolo, A. Mafficini, P. Capelli, R. T. Lawlor, A. Ruzzenente, A. Guglielmi, G. Tortora, F. de Braud, A. Scarpa, W. Jarnagin, D. Klimstra, R. Karchin, V. E. Velculescu, R. H. Hruban, B. Vogelstein, K. W. Kinzler, N. Papadopoulos, L. D. Wood, Exome sequencing identifies frequent inactivating mutations in *BAP1*, *ARID1A* and *PBRM1* in intrahepatic cholangiocarcinomas. *Nat. Genet.* **45**, 1470–1473 (2013).
55. W. Gao, W. Li, T. Xiao, X. S. Liu, W. G. Kaelin Jr., Inactivation of the PBRM1 tumor suppressor gene amplifies the HIF-response in $VHL^{-/-}$ clear cell renal carcinoma. *Proc. Natl. Acad. Sci. U.S.A.* **114**, 1027–1032 (2017).
56. X. Zhuang, D. P. Veltri, E. O. Long, Genome-wide CRISPR screen reveals cancer cell resistance to nk cells induced by NK-derived IFN-γ. *Front. Immunol.* **10**, 2879 (2019).
57. A. J. Freeman, S. J. Vervoort, K. M. Ramsbottom, M. J. Kelly, J. Michie, L. Pijpers, R. W. Johnstone, C. J. Kearney, J. Oliaro, Natural killer cells suppress T cell-associated tumor immune evasion. *Cell Rep.* **28**, 2784–2794.e5 (2019).
58. M. F. Pech, L. E. Fong, J. E. Villalta, L. J. Chan, S. Kharbanda, J. J. O'Brien, F. E. McAllister, A. J. Firestone, C. H. Jan, J. Settleman, Systematic identification of cancer cell vulnerabilities to natural killer cell-mediated immune surveillance. *eLife* **8**, e47362 (2019).
59. D. G. Gamage, T. L. Hendrickson, GPI transamidase and GPI anchored proteins: Oncogenes and biomarkers for cancer. *Crit. Rev. Biochem. Mol. Biol.* **48**, 446–464 (2013).
60. B. Langmead, C. Trapnell, M. Pop, S. L. Salzberg, Ultrafast and memory-efficient alignment of short DNA sequences to the human genome. *Genome Biol.* **10**, R25 (2009).
61. A. R. Quinlan, I. M. Hall, BEDTools: A flexible suite of utilities for comparing genomic features. *Bioinformatics* **26**, 841–842 (2010).
62. L. T. Jae, M. Raaben, M. Riemersma, E. van Beusekom, V. A. Blomen, A. Velds, R. M. Kerkhoven, J. E. Carette, H. Topaloglu, P. Meinecke, M. W. Wessels, D. J. Lefeber, S. P. Whelan, H. van Bokhoven, T. R. Brummelkamp, Deciphering the glycosylome of dystroglycanopathies using haploid screens for lassa virus entry. *Science* **340**, 479–483 (2013).
63. F. A. Ran, P. D. Hsu, J. Wright, V. Agarwala, D. A. Scott, F. Zhang, Genome engineering using the CRISPR-Cas9 system. *Nat. Protoc.* **8**, 2281–2308 (2013).
64. D. R. Gulbranson, E. M. Davis, B. A. Demmitt, Y. Ouyang, Y. Ye, H. Yu, J. Shen, RABIF/MSS4 is a Rab-stabilizing holdase chaperone required for GLUT4 exocytosis. *Proc. Natl. Acad. Sci. U.S.A.* **114**, E8224–E8233 (2017).
65. B. L. Menasche, L. Crisman, D. R. Gulbranson, E. M. Davis, H. Yu, J. Shen, Fluorescence Activated Cell Sorting (FACS) in genome-wide genetic screening of membrane trafficking. *Curr. Protoc. Cell Biol.* **82**, e68 (2019).
66. D. R. Gulbranson, L. Crisman, M. Lee, Y. Ouyang, B. L. Menasche, B. A. Demmitt, C. Wan, T. Nomura, Y. Ye, H. Yu, J. Shen, AAGAB controls AP2 adaptor assembly in clathrin-mediated endocytosis. *Dev. Cell* **50**, 436–446.e5 (2019).

Acknowledgments: We thank C. Dinarello, W. Gao, X. Liu, C. Detweiler, L. Lenz, and B. Weaver for advice or reagents. We thank L. Crisman and I. Datta for comments on the manuscript. **Funding:** This work was financially supported by grants from NIH (GM126960, AG061829, and DK124431 to J.S.; AI128443 to S.L.; AI135473 to H.Y.; GM088759 to B.L.M. and E.M.D.), a Postdoctoral Fellowship from the Postdoctoral Overseas Training Program at Beijing University of Chinese Medicine (S.W.), and seed grants from the Cancer Center and Linda Crnic Institute at University of Colorado (J.S.). Publication of this article was partially funded by the University of Colorado Boulder Libraries Open Access Fund. **Author contributions:** B.L.M., E.M.D., and J.S. designed the study. B.L.M., E.M.D., S.W., Y.O., and S.L. performed the experiments. B.L.M., E.M.D., S.W., S.L., H.Y., and J.S. analyzed the results and wrote the manuscript. All the authors contributed to the overall scientific interpretation and edited the manuscript. **Competing interests:** The authors declare that they have no competing interests. **Data and materials availability:** All data needed to evaluate the conclusions in the paper are present in the paper and/or the Supplementary Materials. Additional data related to this paper may be requested from the authors. All work was carried out at University of Colorado.

Submitted 18 April 2020
Accepted 14 October 2020
Published 27 November 2020
10.1126/sciadv.abc3243

Citation: B. L. Menasche, E. M. Davis, S. Wang, Y. Ouyang, S. Li, H. Yu, J. Shen, PBRM1 and the glycosylphosphatidylinositol biosynthetic pathway promote tumor killing mediated by MHC-unrestricted cytotoxic lymphocytes. *Sci. Adv.* **6**, eabc3243 (2020).